Structural and Dynamic Aspects of Hydration of $HAsO_4^{-2}$: An *ab initio* QMCF MD Simulation

Anirban Bhattacharjee, Andreas B. Pribil, Len Herald V. Lim, Thomas S. Hofer, Bernhard R. Randolf, and Bernd M. Rode*

Theoretical Chemistry Division Institute of General, Inorganic and Theoretical Chemistry, University of Innsbruck, Innrain 52a, A-6020 Innsbruck, Austria

Received: December 15, 2009; Revised Manuscript Received: February 8, 2010

An *ab initio* quantum mechanical charge field simulation has been carried out in order to obtain molecular level insight into the hydration behavior of $HAsO_4^{-2}$, one of the major biologically active components of As(V) oxoanion in neutral to slightly alkaline aqueous medium. Moreover, a geometrical definition of hydrogen bonding has been used to probe and characterize both solute−solvent and solvent−solvent hydrogen bonding present in the system. The asymmetry of the anion induced by the protonation of one of the oxygens of the arsenate anion causes rather irregular hydration structure. The nonprotonated oxygen atoms preferably form relatively stable hydrogen bonds with two to three water molecules in their vicinity, while the protonated oxygen forms one or two hydrogen bonds, weaker than water−water hydrogen bonds. The two types of As−O distances obtained from the simulation (1.68 and 1.78 Å for the protonated and nonprotonated oxygens, respectively) are in good agreement with the experimental data. The two types of As−O stretching frequencies obtained from the simulation (855 and 660 cm^{-1} reproduce well the experimental ATR-FTIR results (859 and 680−700 cm^{-1}).

1. Introduction

The arsenic contamination of groundwater has become one of the most well-known health hazards of the present time.[1,2] The monoprotonated arsenate, i.e., $HAsO_4^{-2}$, is one of the major species containing As(V) in neutral and slightly basic medium.[3,4] The nonprotonated form only exists in strongly alkaline solution. The removal of arsenate and protonated arsenate species from water is of particular interest and crucial in relation to the solution of the worldwide drinking water crisis.[5] Several studies aiming at the development of such techniques have been carried out.[5] A thorough understanding of the solution behavior of this ion in water will be a great help for any such industrial or technical processes involving it, apart from the theoretical relevance of such work. From the theoretical point of view, this particular system offers a challenge because of the difficulties encountered when constructing the solute−solvent multisite potentials which are necessary for classical and/or QM/MM MD studies.[6] However, the novel QMCF-MD approach does not require any such solute−solvent potentials.[7,8] This particular method has been successfully employed for oxoanions[9] (e.g., sulfate,[10,11] phosphate,[12] bicarbonate[13]) and has proven to be quite efficient in probing the structural aspects as well as reproducing spectral information obtained experimentally. AsO_4^{-3} readily hydrolyses in water, forming the main species $HAsO_4^{-2}$.[3,4] By this process, structural irregularities are induced, which have been probed spectroscopically.[4] This particular aspect and its consequences for hydration structure and dynamics have thus been a subject of the present work.

2. Methods

In the QMCF-MD framework, the system of interest is divided into three regions: the chemically most relevant region consisting of a core and a layer region is treated by a quantum mechanical technique, and the remaining part of the system, the MM region, is described in terms of classical mechanics. This procedure has proven efficient to account for complex electronic effects, such as charge transfer and polarization in the wider vicinity of the solute.[7,8] Unlike the conventional QM/MM framework, the QMCF approach has the advantage of not requiring solute−solvent potentials,[7,8] as non-Coulombic interactions between solute and solvent become insignificant if a sufficiently large layer region containing only solvent molecules is provided. Solvent particles close to the center, e.g., the first shell ligands of an ion, are included in the core region. For solvent molecules residing in the layer region, both non-Coulombics and Coulombics must be evaluated, as the interatomic distances are not so large. This, however, requires only the evaluation of the solvent−solvent non-Coulombic interactions, for which the same potential can be applied as for the MM particles. The layer region ensures by its QM treatment a sufficient accuracy for intershell boundary and exchange processes as well. In order to obtain a better description of the influence of surrounding solvent molecules on the quantum mechanical region, the point charges of all MM particles (in accordance with the respective MM model) are included in the core Hamiltonian by a perturbation term. Because of the changing positions of the MM point charges throughout the simulation, the QM region finds itself embedded in a continuously fluctuating chargefield.[7,8] The details of the methodology have been elaborately described elsewhere.[7,8]

The partial charges assigned to the MM particles employed for embedding were taken in accordance with the flexible BJH−CF2 water model[14,15] which was utilized to describe the MM water molecules throughout the simulation. The charges are −0.65966 and 0.32983 unit charges for oxygen and hydrogen, respectively. The partial charges for the atoms inside the QM regions were obtained in every simulation step using

* Corresponding author. E-mail: Bernd.M.Rode@uibk.ac.at. Phone: +43-512-507-5160. Fax: +43-512-507-2714.

10.1021/jp911860y
Published on Web 03/01/2010

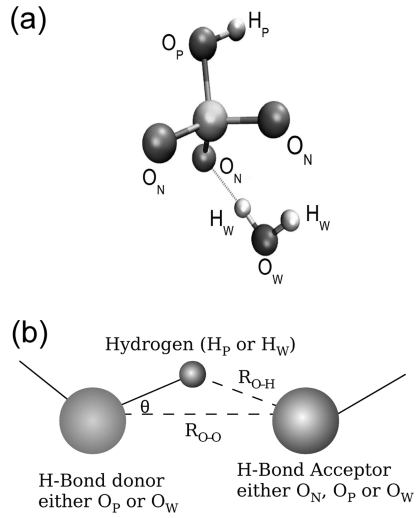

Figure 1. (a) Nomenclature of different nonequivalent interacting sites. (b) Geometric definition of hydrogen bonding using R_{OH}, R_{OO}, and θ parameters (for cutoff values, see text).

Mulliken population analysis[16,17] for the evaluation of the QM-MM Coulombic forces. An important aspect of the study is the choice of basis sets. The cc-PVDZ-pp basis set[18] has been chosen for arsenic, as it has been successfully used in a previous simulation involving As(III).[19] DZP(Dunning)[20] basis sets were used for hydrogen and oxygen after a careful test of their reliability for the description of anions in water, in particular phosphate, sulfate, and perchlorate[12,10,9] employing besides HF also the MP/2, CCSD, and B3LYP density function level in calculations of small anion−water clusters. In this context, also the influence of diffuse functions was tested and found negligible. Differences in interactions and H bond distances between HF and *ab initio* correlated methods proved small enough to accept HF with DZP basis sets as a suitable compromise between accuracy and computational effort and as advantageous compared to the DFT functional.

For the convenience of describing the solvation scenario clearly, different types of nonequivalent interacting sites have been defined (cf., Figure 1a):

- The water oxygen and hydrogen O_W and H_W.
- The three nonprotonated oxygens of hydrogen arsenate ion as O_N.
- The protonated oxygen of the anion as O_P.
- The hydrogen of the OH group of $HAsO_4^{-2}$ as H_P.

The solvent dynamics within and between the different hydration shells were analyzed via mean residence time (τ) calculations using the direct method.[21]

The different types of hydrogen bonds present in the system were probed using the pure geometrical definition, which involves three parameters: R_{OH}, R_{OO}, and θ, described in Figure 1. The upper bounds for the parameter values were chosen as $R_{OH} = 2.5$ Å, $R_{OO} = 3.3$ Å, and $\theta = 30°$, based on neat water classical simulations using the BJH−CF2 model.[14,22] Similar cutoff values for the O_N−water and O_P−water hydrogen bonds were chosen based on the first minima appearing in the corresponding radial distribution functions, as it has been done for systems like solvated bicarbonate,[13] DMSO/water,[23] etc. The dynamic behavior of such hydrogen bonds was characterized in terms of a time correlation function $C_{HB}(\tau)$.[24,25] $C_{HB}(\tau)$ is the intermittent hydrogen bond time correlation function defined as

$$C_{HB}(\tau) = \frac{\langle H(t)\cdot H(t+\tau)\rangle}{\langle H(t)\cdot H(t)\rangle} \quad (1)$$

where $H(t)$ and $H(t + \tau)$ have a value of 1 if a tagged group of atoms are hydrogen bonded at time t or $t + \tau$, respectively, and 0, otherwise. For a given triad of atoms in an arrangement as shown in Figure 1b to be considered as hydrogen bonded, all three parameters (R_{OH}, R_{OO}, and θ as shown in the figure) should attain values lower than the respective upper bounds simultaneously (which are essentially R^c_{OO}, R^c_{OH}, θ^c).

2.1. Simulation Protocol. The simulation of one $HAsO_4^{-2}$ in a 999 water box was started at 298.15 K, using the Berendsen algorithm for thermostatization;[26] the long-range Coulombics were accounted for by the reaction field method. The time step used for the simulation was 0.2 fs, and trajectories were recorded every fifth step. The radius of the core region was taken as 4.0 Å, and that of the layer region, as 6.6 Å. A smoothing function[7,8] was applied between 6.4 and 6.6 Å to ensure a continuous transition of solvent molecules between the QM and MM region. As the best compromise between accuracy and computational demand,[19] the Hartree−Fock level was used for the core and layer region.

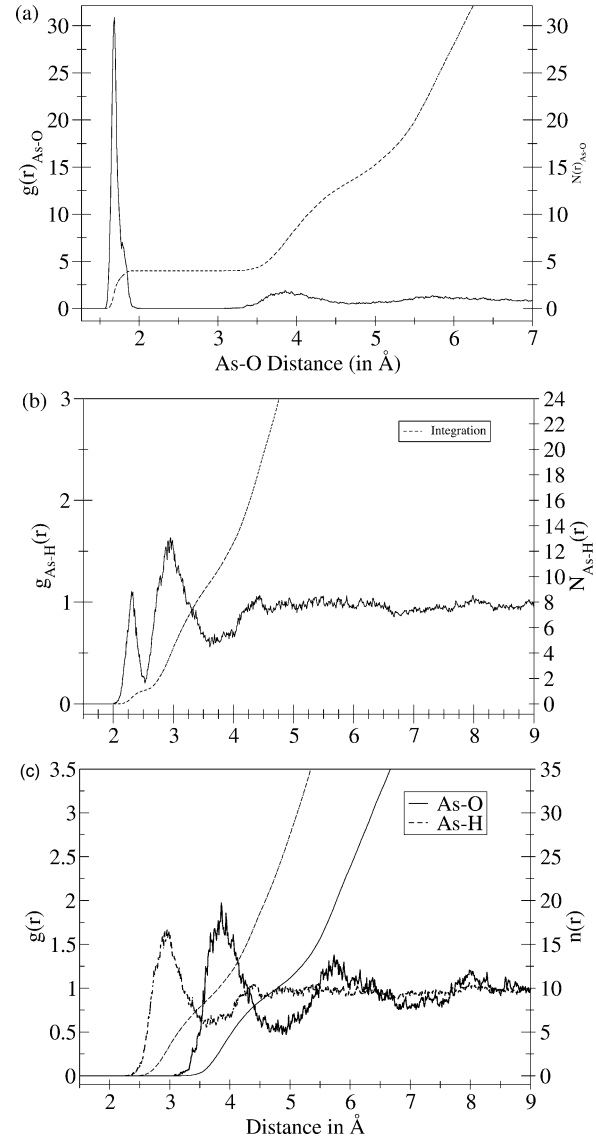

Figure 2. Radial distribution functions for (a) As−O and (b) As−H including the intramolecular peak and (c) As−O and As−H excluding the intramolecular peak.

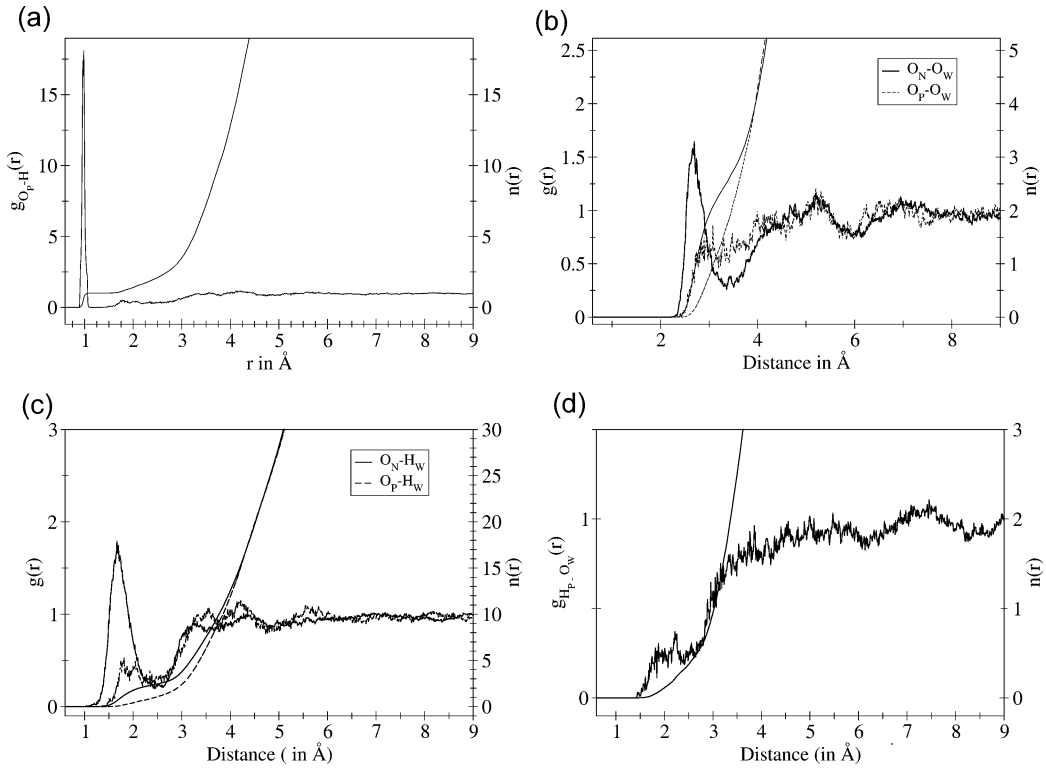

Figure 3. (a) Overall O_P-H radial distribution functions including the intramolecular peak. (b) O_N-O_W and O_P-O_W radial distribution functions. (c) O_N-H_W and O_P-H_W radial distribution functions. (d) H_P-O_W radial distribution functions.

3. Results and Discussion

3.1. Radial Distributions. The first approach to characterize the solvation behavior of $HAsO_4^{-2}$ was based on all relevant radial distribution functions.

The As−O and As−H overall radial distributions are displayed in Figure 2a and b. The As−O distribution starts at 0.93 Å followed by a pair of overlapping peaks at 1.68 and 1.78 Å, respectively, one being approximately 3 times larger than the other. They can be assigned to the two types of oxygen in the anionic solute. The shorter distance corresponds to the three nonprotonated oxygen atoms in the hydrogen arsenate anion and the longer one to the protonated oxygen. Interestingly, the results show that the As−O distances for the oxygens do not differ much from the experimental distance obtained for $Na_2HAsO_4,7H_2O$ crystals[27] (1.66 and 1.74 Å, respectively). The As−H radial distribution (depicted in Figure 2b) shows the first peak around 2.32 Å resulting from hydrogen attached to one of the oxygen atoms.

Figure 2c shows the same As−O and As−H radial distribution functions excluding the intramolecular peaks. Thus, it essentially describes the probability of finding the water oxygen and hydrogen atoms at different distances from the central As atom. From both the As−O and As−H RDF, the first hydration shell is clearly visible. The second hydration shell is not so pronounced, especially in the As−H radial distribution plot. The first hydration shell peak for the As−O radial distribution appears at 3.85 Å followed by a minimum at around 4.75 Å. The integration of the radial distribution yields the average number of ∼10 water oxygens in the first shell. In the case of As−H, the distribution starts from 2.27 Å and reaches a maximum around 2.94 Å followed by a minimum around 3.76 Å. The integration of the RDF also yields an average coordination number of ∼10. The radial distribution of hydrogen atoms near the protonated oxygen atom shows a very sharp peak at 0.978 Å (Figure 3a) which corresponds to the O−H bond and is almost the same as that obtained from the neutron diffraction experiment for the $Na_2HAsO_4,7H_2O$ crystals (0.978 Å[27]).

TABLE 1: Maxima r_M and Minima r_m of the Radial Distribution Function in Å and Average Coordination Number of the Respective Shells for the All Radial Distribution

	r_{M1}	r_{m1}	r_{M2}	r_{m2}	$CN_{av,1}$	$CN_{av,2}$
current simulation:						
As−O(including intra)	1.68, 1.78	3.07	3.85	4.75	4.0	9.8
As−H(including intra)	2.32	2.51	2.96	3.6	1.0	9.9
O_N-H_W	1.67	2.54			2.53	
O_P-H_W	1.82	2.53			1.1	
O_N-O_W	2.69	3.35			2.5	
O_P-O_W					1.1	

Figure 3b and c describes the radial distributions of water oxygens and hydrogens around the nonprotonated and protonated arsenate oxygen atoms (O_N and O_P). The O_N-O_W RDF starts at 2.2 Å and shows a clear peak around 2.67 Å followed by a minimum at 3.35 Å. For the O_P-O_W radial distribution, the first peak is not so pronounced (cf., Figure 3b). None of the radial distributions indicate the presence of a second hydration shell. The O_N-H_W radial distribution shows a single peak at 1.67 Å, while the O_P-H_W shows two weak peaks at 1.8 and 2.0 Å, indicating a relatively weak interaction with neighboring waters. The integration of the radial distributions O_N-O_W and O_N-H_W results in a coordination number of 2.5.

The H_P-O_W RDF (Figure 3d) shows hydrogen bonding at a distance of ∼2.0 Å, not evenly distributed and giving an integration value of only 0.5. This means that the hydroxyl group of biarsenate is not a favored place for binding solvent molecules. All of the information obtained from the RDFs has been summarized in Table 1.

3.2. Solvent Coordination and Hydrogen Bonding. From the radial distribution functions (RDFs), it has been recognized that the influence of the ion on the solvent structure extends

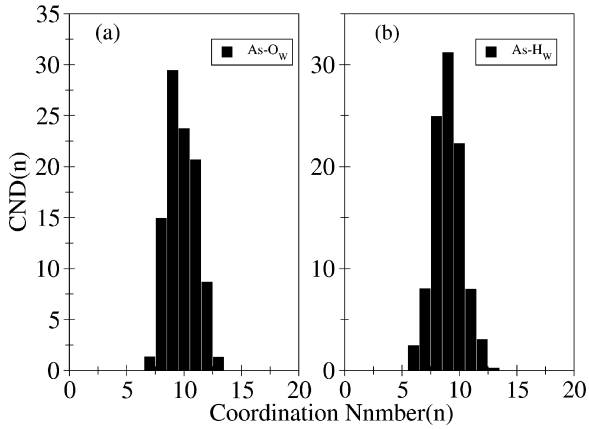

Figure 4. Coordination number distribution for the first hydration shell.

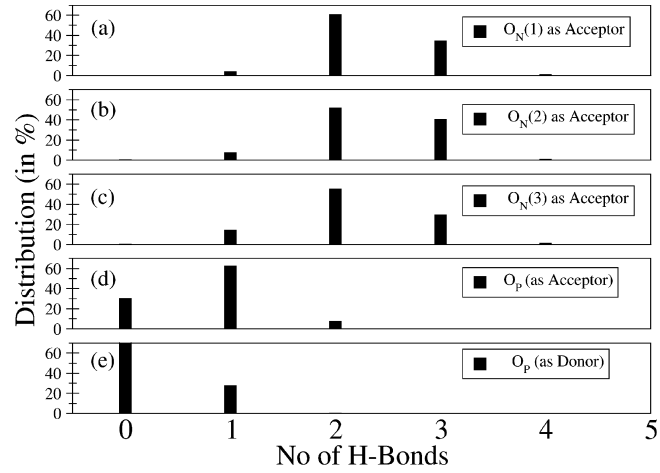

Figure 6. Distribution of the number of hydrogen bonds formed by the different possible sites in the hydrogen-arsenate ion: (a−c) the three O_N sites, (d) the O_P site acting as a hydrogen bond acceptor from water, and (e) the O_P site acting as a hydrogen bond donor via its hydrogen (H_P).

only to one hydration shell. To obtain detailed coordination properties, we have calculated the distribution of hydrogen and oxygen atoms in the first hydration sphere with respect to the central As atom. Figure 4 shows this distribution. The total number of oxygen atoms in the first hydration shell varies from 6 to 13 with a maximum of 9 (29%). The H_W distribution ranges from 6 to 13 with 9 as the most probable value (32%). From these distributions, one can conclude that the hydrogen bonds formed between water and O_P, O_N, and H_P sites primarily involve one hydrogen of a water at a time. However, as there are different types of interaction sites in $HAsO_4^{-2}$, a further evaluation appeared necessary. Therefore, the distribution of the number of O_W and H_W within the first shell boundaries has been evaluated for O_N and O_P separately, as shown in Figure 5. The distributions are similar for the nonprotonated oxygens of the ion which preferably coordinate with two to three water molecules, while the protonated one shows a preference for one to two water molecules.

Using the geometric definition, the distributions of the number of hydrogen bonds formed by different sites has been evaluated and is displayed in Figure 6. For the three nonprotonated oxygens, the preferred number of hydrogen bonds varies within the range of two to three with two having the highest percentage. A very minor percentage of configurations form four hydrogen bonds. Interestingly, the O_N-H_W coordination number distributions have a reverse trend as coordination number 3 is preferred over 2, which may lead to the conclusion that some contribution could stem from the hydrogen of a water which is bonded to a neighboring O_N. The site O_P has the probability of forming hydrogen bonds either with a hydrogen of a neighboring water molecule or via the hydrogen (H_P) attached to itself to the oxygens of the solvent water. The plots shown in Figure 6d and e show that the number of hydrogen bonds formed either way is lower than that of the nonprotonated oxygens. The preferred number of hydrogen bonds for O_P with water hydrogens is 1, while the same for the attached hydrogen with the water oxygen is 0, which means that the site O_P is more likely to form hydrogen bonds with water hydrogens than with the water oxygens via the proton attached to it (H_P).

3.3. Intramolecular Structure and Spectral Analysis. The intramolecular radial distribution functions have been calculated. The mean distance between O_P and O_N (2.73 Å) is significantly shorter than that between O_N and O_N (2.81 Å). A similar effect is visible in the distributions of the angles O_N-As-O_N and O_P-As-O_N differing in their peak by 10° (103 and 113°, respectively).

From the O_N-H_W RDF, it is clear that no intramolecular hydrogen is formed. However, from a careful visual observation,

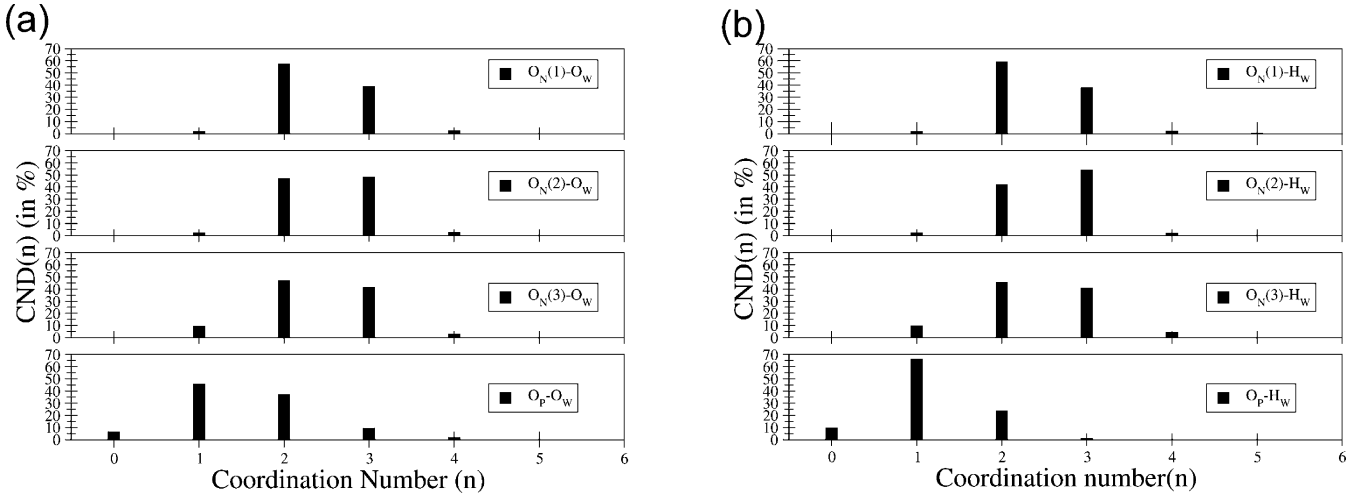

Figure 5. (a) Distribution of the number of O_W for the first solvation shell of O_P and O_N. (b) Distribution of the number of H_W for the first solvation shell of O_P and O_N.

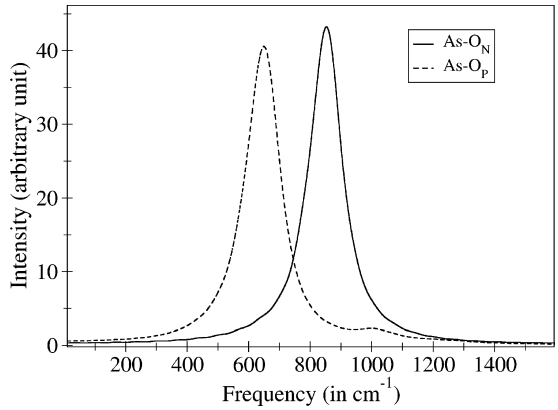

Figure 7. Power spectrum for the As−O_P and As−O_N stretching modes obtained from the Fourier transformation of the velocity autocorrelation functions.

TABLE 2: Mean Residence Time τ in ps, Number of Accounted Ligand Exchange Events N_{ex} per 10 ps, and Sustainability of Migration Process S_{ex} to/from the First and Second Hydration Shell for a t^* Value of 0.0 and 0.5 ps

	N_{ex}^0/10 ps	$\tau^{0.0}$	$N_{ex}^{0.5/10ps}$	$\tau^{0.5}$	S_{ex}	$R_{ex}(1/S_{ex})$
first hydration shell						
$HAsO_4^{-2}$	217.39	0.44	52.3	1.86	0.24	4.16
water		0.2		1.7	0.09	11.2

it has been found that whenever the H_P gets close to O_N the number of water molecules hydrogen bonded to O_N decreases, but such configurations are rare.

The power spectra for As−O_N and As−O_P have been separately calculated using the normal coordinate analysis[28] and are displayed in Figure 7. The average frequencies of the As−O_P and As−O_N stretching motions are 660 and 855 cm^{-1}, respectively. The results are in good agreement with the experimental values obtained from ATR-FTIR (attenuated total reflectance Fourier transform infrared) studies[4] (680−700 and 859 cm^{-1}), thus validating the accuracy and efficiency of the quantum mechanical simulations.

3.4. Dynamics. From the radial distribution functions, it can be deduced that there are numerous exchanges of water molecules between the first hydration shell and the bulk. The mean residence time for the first shell water ligands, calculated by the direct method, is 1.86 ps which is slightly larger than that for the pure water (cf. Table 2) but considerably lower than that of the oxoanions PO_4^{-3} (3.9)[12] and SO_4^{-2} (2.6).[10] These values were accounted for exchange processes lasting for $t^* \geq 0.5$ ps.[21] Comparison with the data obtained with a t^* value of 0.0 are described in Table 2, which also contains the S_{ex} and R_{ex} values which essentially characterize the sustainability of the ligand exchanges. The R_{ex} value of 4.16 indicates that more than four attempts are needed to achieve one successful exchange.[21]

The number of hydrogen bonds formed by the O_N atoms varies from two to three, and both of these configurations are relatively stable. The configurations with four hydrogen bonds are transient (lasting only up to 30−50 fs) and normally occur as an intermediate of an associative water replacement reaction around the O_N sites. Figure 8 illustrates such intermediate species. There is some kind of steric competition of water ligands binding to site O_P via hydrogen. Most of the time, when O_P acts as a hydrogen bond acceptor, it becomes difficult for another water oxygen to form a hydrogen bond with the H_P site, which is reflected in the quite minor appearance of such coordination.

Finally, different types of hydrogen bonds present in the system will be characterized in terms of their dynamic properties. The dynamical parameter C_{HB} as defined in the Methods section is used to describe the decay pattern. A steep initial gradient in the decay curve of $C_{HB}(\tau)$ can be attributed to fast temporary cleavage of hydrogen bonds resulting from orientational changes. Eventually, this effect merges with the translational diffusion, which breaks hydrogen bonds through loss of favorable contact distances. Thus, $C_{HB}(\tau)$ which is basically a time correlation function serves as a convenient tool to explore the coupled dynamical mechanism of hydrogen bond decay. Unfortunately, the simulation time is not long enough to have sufficient sampling points to calculate the hydrogen bond lifetime accurately, but it can be used to characterize the different kinds of hydrogen bonds present in the system. For a simplified approach, one can say that the faster the decay curve approaches zero, the less stable are the corresponding hydrogen bonds. This provides a mean of comparing the nature of hydrogen bonds and also to probe the effect of hydrogen bonding in the vicinity of the solute compared to that in the bulk. As can be seen from

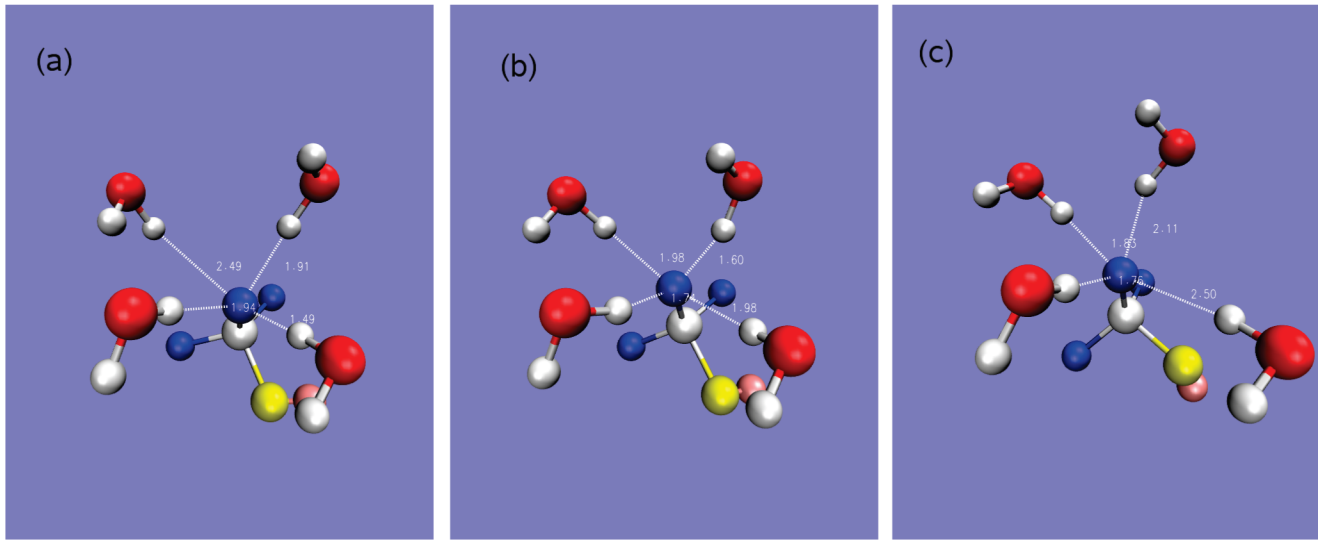

Figure 8. Snapshots depicting an event where two configurations (a and c) with three hydrogen bonds with a selected O_N move from one to the other via a transient intermediate where the selected O_N atom forms four hydrogen bonds with four different water molecules (b).

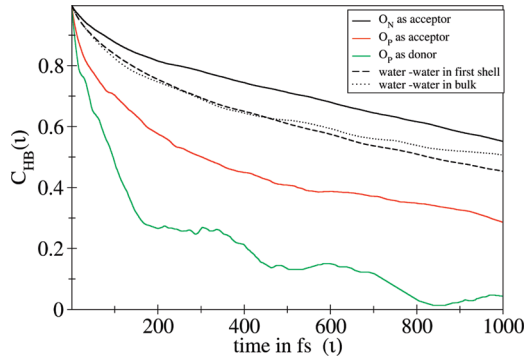

Figure 9. Comparison of the time correlation function $C_{HB}(\tau)$ for the different types of hydrogen bonding present in the system.

the plot shown in Figure 9, the most stable hydrogen bond (i.e., the slowest decaying one) exists between the O_N atoms and water, being stronger than the water−water hydrogen bonds in the bulk and also in the first solvation shell. O_P−water hydrogen bonds with O_P acting as an acceptor are by far more stable than the hydrogen bonds of the H_P donor. Both of them are weaker than the water−water hydrogen bonds in the bulk, which essentially means that the $HAsO_4^{-2}$ ion acts as a structure breaker and a structure former simultaneously based on which site of it is interacting with water. As the nonprotonated oxygens dominate, overall, the ion can be considered as a structure former, which agrees with the MRT calculations presented above. The difference in the decay pattern of the water−water hydrogen bonds between the bulk and first hydration shell water molecules is not so pronounced. Apparently, the water−water hydrogen bonds in the vicinity of the solute are not considerably affected by the presence of the solute.

4. Conclusion

The reliability of the QMCF MD simulation technique could be validated by the good agreement with all available spectroscopic results, and its straightforward applicability without the need for solute−solvent potentials and advantages related to this point could be demonstrated clearly for a composite anion with relatively low symmetry. The current study has thus provided detailed insight into the solvation structure of the ion in solution and has, in particular, enabled a differentiation between the types of hydrogen bonds formed between donor and acceptor sites of the anion and water. Of special interest in this context is the formation of stronger H bonds by the oxygen atoms of the ion compared to the hydrogen of the OH group, thus giving valuable hints toward the reactivity of different sites of the hydrogen arsenate ion in aqueous solution. Together with the rapid hydrolysis of the arsenate ion AsO_4^{-3} leading to the stable hydrogen arsenate studied here,[29] the QMCF MD results have thus provided significant new knowledge about the aqueous chemistry of these ions.

Acknowledgment. Financial support from the Austrian Science Foundation (FWF) and ASEAN-European Academic University Network technology grants from the Austrian Ministry of Science and Research for A.B. and L.H.V.L. is gratefully acknowledged.

References and Notes

(1) Gupta, V. K.; Saini, V. K.; Jain, N. *J. Colloid Interface Sci.* **2005**, *288*, 55–60.
(2) Pontius, F. W.; Brown, K. G.; Chen, C. J. *J.—Am. Water Works Assoc.* **1994**, *86*, 52–63.
(3) Cotton, F. A.; Wilkinson, G.; Murillo, C. A.; Bochmann, M. *Advanced Inorganic Chemistry*, 6th ed.; Wiley-Interscience: 1999.
(4) Myneni, S. C. B.; Traina, S. J.; Logan, T. J. *Geochim. Cosmochim. Acta* **1998**, *62*, 3285–3300.
(5) Bissen, M.; Frimmel, F. H. *Acta Hydrochim. Hydrobiol.* **2003**, *31*, 97–107.
(6) Hofer, T. S.; Randolf, B. R.; Rode, B. M. In *Solvation Effects on Molecules and Biomolecules*; Springer: Heidelberg, Germany, 2008.
(7) Rode, B. M.; Hofer, T. S.; Randolf, B. R.; Schwenk, C. F.; Xenides, D.; Vchirawongkwin, V. *Theor. Chim. Acta* **2006**, *115*, 77.
(8) Rode, B. M.; Hofer, T. S.; Randolf, B. R.; Pribil, A. B.; Vchirawongkwin, V. Ab initio quantum mechanical charge field (qmcf) simulations: New horizons in solution chemistry. In *Trends and Perspectives in Modern Computational Science*; G. Maroulis, T. S., Ed.; International Science Publishers (VSP): Leiden, The Netherlands, 2006; p 441.
(9) Simos, T. E., Ed. *Structure and Dynamics of Composite Anions in Aqueous Solution*; American Institute of Physics (AIP): New York, 2007.
(10) Vchirawongkwin, V.; Persson, I.; Rode, B. M. *J. Phys. Chem. B* **2007**, *111*, 4150.
(11) Vchirawongkwin, V.; Rode, B. M. *Chem. Phys. Lett.* **2007**, *443*, 152–157.
(12) Pribil, A. B.; Hofer, T. S.; Randolf, B. R.; Rode, B. M. *J. Comput. Chem.* **2008**, *29* (14), 2330–2334.
(13) Vchirawongkwin, V.; Pribil, A. B.; Rode, B. M. *J. Comput. Chem.* **2009**.
(14) Stillinger, F. H.; Rahman, A. *J. Chem. Phys.* **1978**, *68* (2), 666–670.
(15) Bopp, P.; Janscó, G.; Heinzinger, K. *Chem. Phys. Lett.* **1983**, *98* (2), 129–133.
(16) Mulliken, R. S. *J. Chem. Phys.* **1955**, *23* (10), 1833–1840.
(17) Mulliken, R. S. *J. Chem. Phys.* **1955**, *23* (10), 1841–1846.
(18) Peterson, K. A. *J. Chem. Phys.* **2003**, *119* (21), 11099.
(19) Bhattacharjee, A.; Hofer, T. S.; Pribil, A. B.; Randolf, B. R.; Rode, B. M. *Chem. Phys. Lett.* **2009**, *473*, 176–178.
(20) Dunning, T. H., Jr. *J. Chem. Phys.* **1970**, *53* (7), 2823–2833.
(21) Hofer, T. S.; Tran, H. T.; Schwenk, C. F.; Rode, B. M. *J. Comput. Chem.* **2004**, *473*, 211–214.
(22) Bopp, P.; Jancso, G.; Heinzinger, K. *Chem. Phys. Lett.* **1983**, *98*, 129–133.
(23) Luzar, A.; Chandler, D. *J. Chem. Phys.* **1993**, *98*, 8160.
(24) Stillinger, F. H. *Science* **1980**, *25*, 451–457.
(25) Luzar, A.; Chandler, D. In *Hydrogen Bond Networks*; Kluwer Academic Publishers: The Netherlands, 1994.
(26) Berendsen, H. J. C.; Postma, J. P. M.; van Gunsteren, W. F.; DiNola, A.; Haak, J. R. *J. Phys. Chem.* **1984**, *81*, 3684–3690.
(27) Ferraris, G.; Jones, J. W.; Yerkess, J. *Acta Crystallogr., Sect. B* **1970**, *26*, 1574.
(28) Bopp, P. *Chem. Phys.* **1986**, *106* (2), 205.
(29) Bhattacharjee, A.; Hofer, T. S.; Pribil, A. B.; Randolf, B. R.; Rode, B. M. *Phys. Chem. Chem. Phys.*, submitted for publication, **2009**.

JP911860Y